

Article

Risk Assessment of Population Loss Posed by Earthquake-Landslide-Debris Flow Disaster Chain: A Case Study in Wenchuan, China

Xiang Han ^{1,2}, Yunhe Yin ^{1,*}, Yuming Wu ³ and Shaohong Wu ^{1,2}

¹ Key Laboratory of Land Surface Pattern and Simulation, Institute of Geographic Sciences and Natural Resources Research, Chinese Academy of Sciences, Beijing 100101, China; hanx.18b@igsnr.ac.cn (X.H.); wush@igsnr.ac.cn (S.W.)

² University of Chinese Academy of Sciences, Beijing 100101, China

³ State Key Laboratory of Resources and Environmental Information Systems, Institute of Geographic Sciences and Natural Resources Research, Chinese Academy of Sciences, Beijing 100101, China; wuym@lreis.ac.cn

* Correspondence: yinyh@igsnr.ac.cn

Abstract: Earthquakes often cause secondary disasters in mountainous areas, forming the typical earthquake-landslide-debris flow disaster chain for a long time that results in a series of losses. It is important to improve the risk assessment method from the perspective of cascading effect of such a disaster chain, by strengthening quantitative research on hazards of the debris flows which are affected by landslide volume and rainstorm intensity. Taking Wenchuan County as an example, the risk assessment method for population loss of the disaster chain is established and the risks are evaluated in this paper. The results show that the population loss risk is 2.59–2.71 people/km² under the scenarios of the Wenchuan Ms8.0 earthquake and four rainstorm intensities. The impacts of landslide and debris flow after the earthquake were long-term and profound. A comparison of risks caused by each element of the chain revealed that the risk associated with the earthquake accounted for the highest proportion, and landslide and debris flow accounted for 38.82–37.18% and 3.42–7.50%, respectively. As the earthquake intensity increases, the total risk posed by the disaster chain increases significantly. The risk caused by the earthquake is the highest in high earthquake intensity zones; while in the lower-intensity zones, landslides and debris flows pose relatively high risks. The risk assessment results were verified through comparison with actual data, indicating that the simulation results are quite consistent with the existing disaster information and that the risk assessment method based on the earthquake-landslide-debris flow cascade process is significant for future risk estimation.

Keywords: risk assessment; disaster chain; population loss; debris flows; Wenchuan



Citation: Han, X.; Yin, Y.; Wu, Y.; Wu, S. Risk Assessment of Population Loss Posed by Earthquake-Landslide-Debris Flow Disaster Chain: A Case Study in Wenchuan, China. *ISPRS Int. J. Geo-Inf.* **2021**, *10*, 363. <https://doi.org/10.3390/ijgi10060363>

Academic Editors: Dean Kyne and Wolfgang Kainz

Received: 31 March 2021

Accepted: 25 May 2021

Published: 28 May 2021

Publisher's Note: MDPI stays neutral with regard to jurisdictional claims in published maps and institutional affiliations.



Copyright: © 2021 by the authors. Licensee MDPI, Basel, Switzerland. This article is an open access article distributed under the terms and conditions of the Creative Commons Attribution (CC BY) license (<https://creativecommons.org/licenses/by/4.0/>).

1. Introduction

Natural disasters have a huge impact on the regional population, economy, resources, and environment [1,2]. Many organizations and regional plans around the world have emphasized the importance of improving natural disaster risk prevention capabilities [3–5]. Earthquakes are one of the main causes of geological disasters, and they can cause huge losses to regional populations [6–9]. A variety of disaster risk prevention measures have been formulated and adopted to reduce future impacts of earthquakes [10]. However, the occurrence of secondary geological disasters such as landslides and debris flows under the influence of great earthquakes may result in severe damage and long-term accumulation [11–15]. Moreover, they are characterized by sudden occurrences and hidden dangers [16]. The prevention and control of these disasters are long-term and difficult, and the risk of population loss posed by these disasters has attracted widespread attention [5,8,9,17].

The earthquake-geological disaster chain is a common manifestation of multiple disasters, and it often causes serious damage due to the indirect strengthening effect of earthquakes that are extensive, persistent, and clustered [18–20]. Great earthquakes can not only cause a large number of landslides, but they can also aggravate the instability of slopes for a long time after the earthquake [7,11,12,21,22]. For example, there were about 5000 landslides in the Haiti earthquake on 12 January 2010 [21], and in the Maule earthquake there were 1226 landslides over an area of 120,500 km² and the rock mass was more fragmented [6]. The asymmetric distribution of inclined fault may lead to differences of damage between hanging wall and footwall [23]. As for the damage distribution, hazards on hanging walls are denser in distribution, wider in scope, and larger in scale, comparing to footwall [12,23,24]. Large-scale landslides on fault-hanging walls generate a large number of loose deposits in the gully or valley, which provide ample sources of loose material for later debris flows under rainstorm scenarios [7,12,25]. When heavy rain falls on mountain torrents with complex geological conditions (such as steep terrain, large slopes, many loose materials, and soft lithology) [7,12], and the critical disaster-causing rainfall threshold is reached, debris flows are easily triggered [12,13,25,26]. The long-term potential threat of landslides and debris flows in earthquake-stricken areas has a very obvious time lag effect [3,27–29], and may be as long as 30 years in Wenchuan [26,30].

The Wenchuan earthquake in 2008 was one of the most destructive earthquakes in China [7,12,13]. It led to a typical earthquake-landslide-debris flow disaster chain based on geological settings of high relief, steep slopes, dense river network, and intense phenomena of erosion [12,13]. The earthquake triggered a large number of landslides and posed major threats to mountain residents, directly leading to the death of more than 20,000 people [31]. The amount and volume of the regional landslides increased after the earthquake, leading to a large amount of material accumulating in the gullies due to the amplification effect of the topography and the impact of river erosion [32,33]. Due to the landslides, the area and volume of the non-compacted materials in the gullies were greatly increased, which contributed to the initiation of debris flows. These debris flows changed from the own channel erosion mode to the source replenishment mode and were prone to be transformed into rainfall-triggered events in the study period, dramatically increasing their frequency and duration [7,26]. Most of the gullies in Wenchuan County have conditions favorable to the formation of debris flows, which has resulted in many catastrophic gully-type debris flows in the years after the Wenchuan earthquake, such as the 8.14 debris flow in Yingxiu in 2010, the 7.10 debris flow in 2013, and the 8.20 debris flow in 2019 [7,34].

Disaster chain risk assessment is a hot topic in multi-disaster research, and it is helpful for risk prevention and control [1,22,35–39]. The disaster risk is dependent on the hazard, vulnerability, and exposure in terms of the population, ecology, and society, which have been widely used to effectively quantify the potential loss [37,40–42]. During the risk assessment process of the earthquake-landslide-debris flow disaster chain, one of the difficult points in such research is the hazard assessment of debris flows in areas affected by earthquake-triggered landslides [20,43–47]. Mathematical analysis and numerical simulation are the main methods used in this research field [20,46]. Mathematical analysis is mainly based on the establishment of an indicator system, including rainfall, topography, lithology, and vegetation, to evaluate the hazards in potential areas [6,44]. The potential path in the gully and the alluvial fan are the potential hazard areas and their ranges are important parts for debris-flow risk assessment [48]. Considering the cascading effect in an earthquake-landslide-debris flow disaster chain, the conditions necessary for the formation of a debris flow in Wenchuan are rainstorms and landslide-triggered non-compacted materials [18,43–46]. Hazard analysis could further consider the influences of these factors and strengthen the expression of factors such as the material source and peak discharge to achieve reliable risk assessment of landslide-generated debris flows.

The risk assessment of population loss posed by disaster chain is an important way to achieve comprehensive disaster prevention and mitigation [6]. In this study, from the perspective of the cascading effect of an earthquake-landslide-debris flow disaster chain in

Wenchuan County, the risk assessment method was improved in terms of the identification and assessment of debris flow hazards under earthquake and rainstorm scenarios, and the quantitative risk assessment of the population loss was conducted to provide a scientific basis for regional seismic geological disaster prevention and management.

2. Study Area and Materials

Wenchuan County (Figure 1) is located on the eastern edge of the Tibetan Plateau, and it is characterized by an altitude of 783–6057 m and a large degree of undulation. The study area is constructed by 9 towns, including Bazhou, Weizhou, Miansi, Gengda, Yingxiu, Xuankou, Shuimo, Sanjiang, and Wolong. The population distribution is relatively sparse, with an average density of 28.22 people/km² in 2015. It is relatively high in Xuankou and Shuimo (60.66 people/km² and 45.15 people/km², respectively). The stratum of Wenchuan County is mainly distributed with Triassic, Devonian, and Proterozoic stratum. The lithology mainly includes magmatic rocks, metamorphic rocks, sandstone, and conglomerate [30]. The Wenchuan-Maoxian fault, Yingxiu-Beichuan fault, and Guanxian-Anxian fault are the main fault zones in Wenchuan. The epicenter of the Wenchuan Ms8.0 earthquake was in Yingxiu. According to the division of the intensity zone by the China Earthquake Administration [11], Yingxiu and Xuankou are located in the XI Intensity Zone, and Bazhou, Miansi, Gengda, Wolong, and Sanjiang are mostly located in the VIII and IX Intensity Zones. The complex geological structure and steep terrain in Wenchuan have led to a large number of landslides and debris flows after earthquakes [7,30].

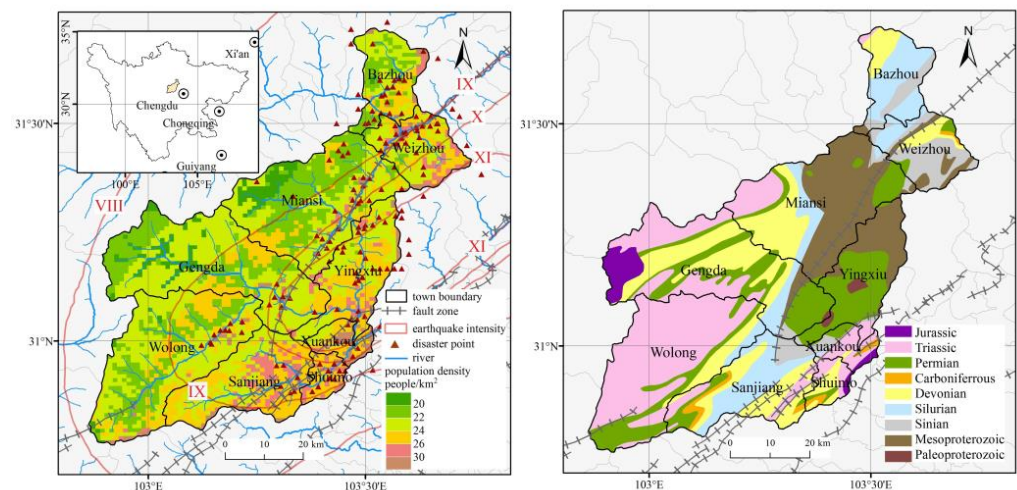


Figure 1. The geographical location of the study area, population distribution, locations of the fault zone and disaster points, and stratigraphic distribution.

The data sources are summarized in Table 1, including the geographical, disaster, and statistical data. The geographical data include the elevation, relief degree, population, geologic map, soil and water erosion, Normalized Difference Vegetation Index (NDVI), Fractional Vegetation Cover (FVC), faults, and human activity index data used to evaluate the debris flow hazards. Soil and water erosion refers to [49] to evaluate and classify the mean soil erosion modulus. The human activity index is based on the interpretation data of remote sensing images and is obtained by converting the construction land area [50]. The disaster data include earthquake intensity, several disaster points, and the corresponding population losses, which are used to analyze the result of the risk assessment. The statistical data include the earthquake-landslide hazards and the population loss vulnerability due to earthquakes, landslides, and debris flows from previous studies.

Table 1. Sources of the data used for the risk assessment of the earthquake-landslide-debris flow disaster chain.

Data Type	Content	Description	Sources
Geographical data	DEM (Digital Elevation Model)	30 m × 30 m grid data	DEM ASTGTM
	Relief degree of land surface	1 km × 1 km grid data	National Earth System Science Data Center
	Spatial distribution of population	1 km × 1 km grid data (2015)	Resource and Environment Science and Data Center
	1:5,000,000 geologic map	Geological group and lithology	China Geological Survey
	Soil erosion and water erosion	300 m × 300 m grid data (2015)	National Tibetan Plateau Data Center
	NDVI	1 km × 1 km grid data (2015)	Resource and Environment Science and Data Center
	FVC	1 km × 1 km grid data (2015)	National Earth System Science Data Center
	Fault	Fault distribution	China Earthquake Administration
Human activity index	Index based on land-use change	National Earth System Science Data Center	
Disaster data	Earthquake intensity	Spatial distribution of intensity of Wenchuan Ms8.0 Earthquake	China Earthquake Administration
	Disaster distribution	Locations of landslide and debris flow points	National Earth System Science Data Center
	Disaster loss	Population loss in Wenchuan Ms8.0 earthquake and several geological disaster points	Statistical Yearbook, Materials, data from reports
Statistical data	Hazard of earthquake-landslide	Probability and aggregation degree of landslides (H_{ls})	[41]
	Vulnerability curves or indexes for different disasters	Vulnerability to earthquakes (V_{eq}):	[51]
		$L_{peop} = 1 / (0.01 + 1.534 \times 10^8 \times 0.13^I)$	
		Vulnerability to landslides (V_{ls}):	[52]
		$C_{max} = 3.681 * V_L^{0.155} \quad R^2 = 0.973$	
		$C_{min} = 0.980 * V_L^{0.122} \quad R^2 = 0.964$	
Vulnerability to debris flows (V_{df}):	[53]		
	Xuankou, 0.3616; Sanjiang, 0.0672; Yinxing, 0.0766; Wolong, 0.0813; Gengda, 0.0819; Caopo, 0.0997; Longxi, 0.1171; Yanmen, 0.1185; Yingxiu, 0.1412; Keku, 0.1552; Miansi, 0.2538; Shuimo, 0.3874; Weizhou, 1.0000		

3. Methods

3.1. Risk Assessment Method for Disaster Chain

The risk assessment method for the disaster chain was used to quantify the potential population loss caused by an earthquake-landslide-debris flow chain under various scenarios in Wenchuan. Among the expressions of various risk assessment methods, it is widely recognized that the risk composition consists of three aspects and is usually defined as

$$R = H \times V \times E \quad (1)$$

where H stands for hazards, indicating the probability of disaster occurrence, and is mainly determined by the scale, intensity, and frequency. V is the vulnerability to a specific hazard intensity, and E is the exposure of the element at risk [54,55]. According to the theory of multi-disaster risk [20,40,41], the expression of the disaster chain risk is the accumulation of the primary disaster risk and the secondary disasters risks:

$$\begin{aligned} R_{dc} &= R_{eq} + R_{ls} + R_{df} = H_{eq}V_{eq}E_{eq} + H_{ls}V_{ls}E_{ls} + H_{df}V_{df}E_{df} \\ &= H_{eq}V_{eq}E_{eq} + H_{ls}V_{ls}(E_{eq} - R_{eq}) + H_{df}V_{df}(E_{ls} - R_{ls}) \end{aligned} \quad (2)$$

where R_{dc} is the risk of population loss posed by the earthquake-landslide-debris flow disaster chain; R_{eq} , R_{ls} , and R_{df} are the risks of the earthquake, landslide, and debris flow in the chain, representing a population loss step by step; V_{eq} , V_{ls} , and V_{df} are the vulnerabilities to population loss caused by the earthquake, landslide, and debris flow in Table 1, respectively; and E_{eq} , E_{ls} , and E_{df} are the population densities in the earthquake, landslide, and debris flow areas, respectively (people/km²). H_{eq} is the hazard posed by the earthquake, which is represented by the Wenchuan Ms8.0 earthquake's intensity in this paper. H_{ls} is the hazard posed by landslides, which was obtained by [41] through the analysis of the probability and movement of landslides (Table 1). H_{df} is the hazard posed by debris flows, which was calculated by constructing an evaluation method and consists of the hazard area and intensity:

$$H_{df} = g[S_{df}(y_{Hls}); y_{Hls}, \dots, y_m] \quad (3)$$

where S_{df} (Figure 2) is the potential hazard area of the debris flow, which is related to a landslide factor; and y represents the factors used to construct the indicator system.

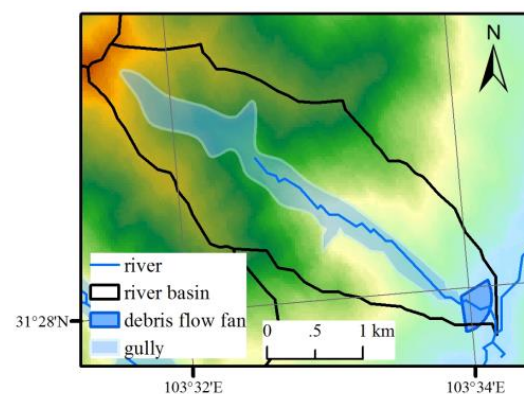


Figure 2. The potential path in the gully and the resultant alluvial fan.

3.2. Hazard Model for a Seismic Landslide-Generated Debris Flow

3.2.1. Method for Delimiting the Hazard Area of the Debris Flow

The S_{df} includes the potential path in the gully (S_{gully}) and the resultant alluvial fan (S_{fan}):

$$S_{df} = S_{gully} + S_{fan} \quad (4)$$

Based on the DEM for Wenchuan, the sub-basins with areas of mostly less than 5 km² were extracted [30]. The study area is dominated by gully-type debris flows that threaten the population after the earthquake [30,56–58]. In each sub-basin, the potential flow paths were mainly determined by the terrain in Wenchuan [26,56–58]. The edges of paths in the gully were detected using the Laplacian of the Gaussian (LOG) operator [59] according to the zero points of the second derivative:

$$S_{gully} = S(LOG) = f \left[-\frac{1}{\pi\sigma^4} \left(1 - \frac{a^2 + b^2}{2\sigma^2} \right) e^{-\frac{a^2 + b^2}{2\sigma^2}} \right] \quad (5)$$

where a and b are the elevation of points and σ is the variance of the pixel in each window. A 3×3 window and a threshold of 1.20 (σ) were used in this study.

The possible debris-flow runout zones on the alluvial fans were predicted using the empirical formula for its radius [48]:

$$S_{fan} = S(L) = 0.05H^{0.43}V_D^{0.28} \quad (6)$$

where L is the maximum accumulation length of the deposition fan (km); H is the elevation difference in the sub-basin (km), and V_D is the volume of the non-compacted materials (10^4 m^3). In this study, an empirical formula was used to estimate V_D [57,60]:

$$V_D = 14.3698A^{0.2456}A_L^{0.2732}H^{0.2798} \quad (7)$$

where A is the area of the sub-basin (km^2) and A_L is the area of the landslide in this basin (km^2).

3.2.2. Hazard Assessment of Seismic Landslide-Generated Debris Flow

In this study, the hazard intensity of the debris flow was estimated using the indicators in the hazard area:

$$H_{df} = y_1w_1 + \dots + y_nw_n \quad (8)$$

The landslide intensity (simulation volume) (y_1), debris flow intensity (peak discharge (y_2) and velocity (y_3), altitude (y_4), relief degree (y_5), degree of basin cutting (y_6), lithology (y_7), distance to the fault (y_8), NDVI (y_9), FVC (y_{10}), soil erosion (y_{11}), water erosion (y_{12}), and human activity index (y_{13}) were selected as the hazard factors for the debris flow and were divided into five levels according to different thresholds and were assigned values of 0.2, 0.4, 0.6, 0.8, or 1.0. w is the weight of each factor, which was synthesized using the Entropy Method (EM) and the Analytic Hierarchy Process (AHP) which need to refer to the explanation of factor weight in the existing research [61–64].

The debris flow intensity (y_2 and y_3) was simulated based on different rainstorm scenarios. The peak discharge is [65]:

$$Q_C = (1 + \phi_C)D_CQ_P = (1 + \phi_C)D_C \times 0.278\phi_iF \quad (9)$$

where Q_C is the peak discharge of the debris flow (m^3/s); Q_P is the peak discharge of clear water (m^3/s); ϕ_C is the correction coefficient of the debris flow; D_C is the obstructive coefficient; ϕ is the peak discharge coefficient of the clear water; F is the area of the basin (km^2), and i is the maximum rainstorm intensity under different scenarios (mm/h) based on the historical rainfall and researches about triggering rainfall of debris flows [66–68].

The velocity of the debris flow is one of the important parameters describing its dynamics. The formula for a sparse debris flow in the southwestern region was adopted [65]:

$$V_C = \frac{1}{\sqrt{\gamma_H\phi + 1}} \frac{1}{n} H_C^{2/3} I_C^{1/2} \quad (10)$$

where V_C is the peak velocity of the debris flow (m/s); γ_H is the density of the solid material in the debris flow (t/m^3), H_C is the hydraulic radius, which can be approximated as the depth of the mud (m); and $1/n$ is the roughness coefficient of the river bed, with a value of 10. I_C is the hydraulic slope of the debris flow and is replaced by the vertical drop ($\%$). The parameters usually vary with rainstorm intensity, and the information in Table 2 is based on experience and previous research [56,69,70].

Table 2. Debris flow parameters under different rainstorm scenarios.

Rainstorm Scenarios (RS)	RS1	RS2	RS3	RS4
i (mm/h)	20	29	35	40
ϕ	0.54	0.63	0.60	0.75
γ_H (t/m^3)	1.697	1.612	1.501	1.416
ϕ_C	0.34	0.44	0.59	0.73
D_C	1.5	1.5	1.5	1.5
H_C (m)	1	2	3	5

3.3. Spatial Statistical and Analysis Methods

This article uses some spatial analysis and statistical tools in GIS. Hydrological tools are used to extract sub-basins based on DEM, and spatial statistics tools are used to analyze regional hazard factors and risks of the disaster chain.

4. Results

4.1. Debris-Flow Hazards in Wenchuan

4.1.1. Classification and Weighting of the Debris Flow Factors

The debris flow factors were counted and divided into five levels (Figure 3). The landslide volume in the sub-basin was mainly $126.89\text{--}2287.66 \times 10^4 \text{ m}^3$, with higher volumes in Gengda, Miansi, and Xuankou. The peak discharge and velocity of the debris flows in the sub-basin under different rainstorm scenarios were classified according to the natural breakpoint method. The peak discharge increases with rainstorm intensity at $78.41 \pm 5.06 \text{ m}^3/\text{s}$ (RS1), $151.09 \pm 9.76 \text{ m}^3/\text{s}$ (RS2), $230.07 \pm 14.86 \text{ m}^3/\text{s}$ (RS3), and $336.99 \pm 21.77 \text{ m}^3/\text{s}$ (RS4); and the velocity increases at $4.61 \pm 0.07 \text{ m/s}$ (RS1), $6.24 \pm 0.10 \text{ m/s}$ (RS2), $7.56 \pm 0.12 \text{ m/s}$ (RS3), and $8.40 \pm 0.13 \text{ m/s}$ (RS4).

The regional average elevation in Wenchuan is 2967 m, with higher elevations in the southwest region. The land relief ranges from 0.55 to 9.22 m, exhibiting an overall downward trend toward the southeast. Based on the GB50218T-2014 (China) engineering rock mass grading standards, the rock masses were divided into five types. The engineering geological group is soft in Xuankou and Shuimo. Soft layers mainly consist of mudstone and shale which are prone to be damaged. In terms of faults, the area within 1000 m of the fault was the most affected by the earthquake and the post-earthquake landslides [12,15,30]. The regional NDVI is 0.024–0.900, and the value is higher than the average in 77.78% of the region. The FVC in the study area is 0.12–0.61, with an average of 0.40. The spatial distributions of the NDVI and FVC both reflect the characteristics of lower vegetation coverage in the higher altitude areas. A total of 13.20% of the region has a soil erosion degree of greater than 8000, and these regions are mainly located in the high-altitude western area. The areas with high water erosion account for 5.61% of the total area and are mainly located in Gengda.

The results of the weight analysis of the hazard factors based on Equation (8) are shown in Table 3. The landslide volume and altitude are relatively higher based on the EM, accounting for 27.29% and 15.01%, respectively. The weights based on the AHP are 11.16%, 10.29%, 14.55%, 28.48%, 1.49%, 2.94%, 4.98%, 8.45%, 2.22%, 2.83%, 5.63%, 2.36%, and 4.61% with a Consistency Index of 0.138 and a Consistency Ratio of 0.08, which means that they pass the consistency test. The comprehensive weights obtained using the two methods indicate that the weight of the landslide volume is highest (20.92%), followed by that of the altitude (21.75%). The comprehensive weights are used in the debris flow hazard assessment.

Table 3. The weights of the debris flow indicators.

Indicators	y_1	y_2	y_3	y_4	y_5	y_6	y_7	y_8	y_9	y_{10}	y_{11}	y_{12}	y_{13}
Weights of EM (%)	27.29	11.98	1.44	15.01	1.05	2.28	4.53	6.95	0.59	4.07	10.02	2.46	12.33
Weights of AHP (%)	14.55	11.16	10.29	28.48	1.49	2.94	4.98	8.45	2.22	2.83	5.63	2.36	4.61
Comprehensive weights (%)	20.92	11.57	5.87	21.75	1.27	2.61	4.75	7.70	1.41	3.45	7.82	2.41	8.47

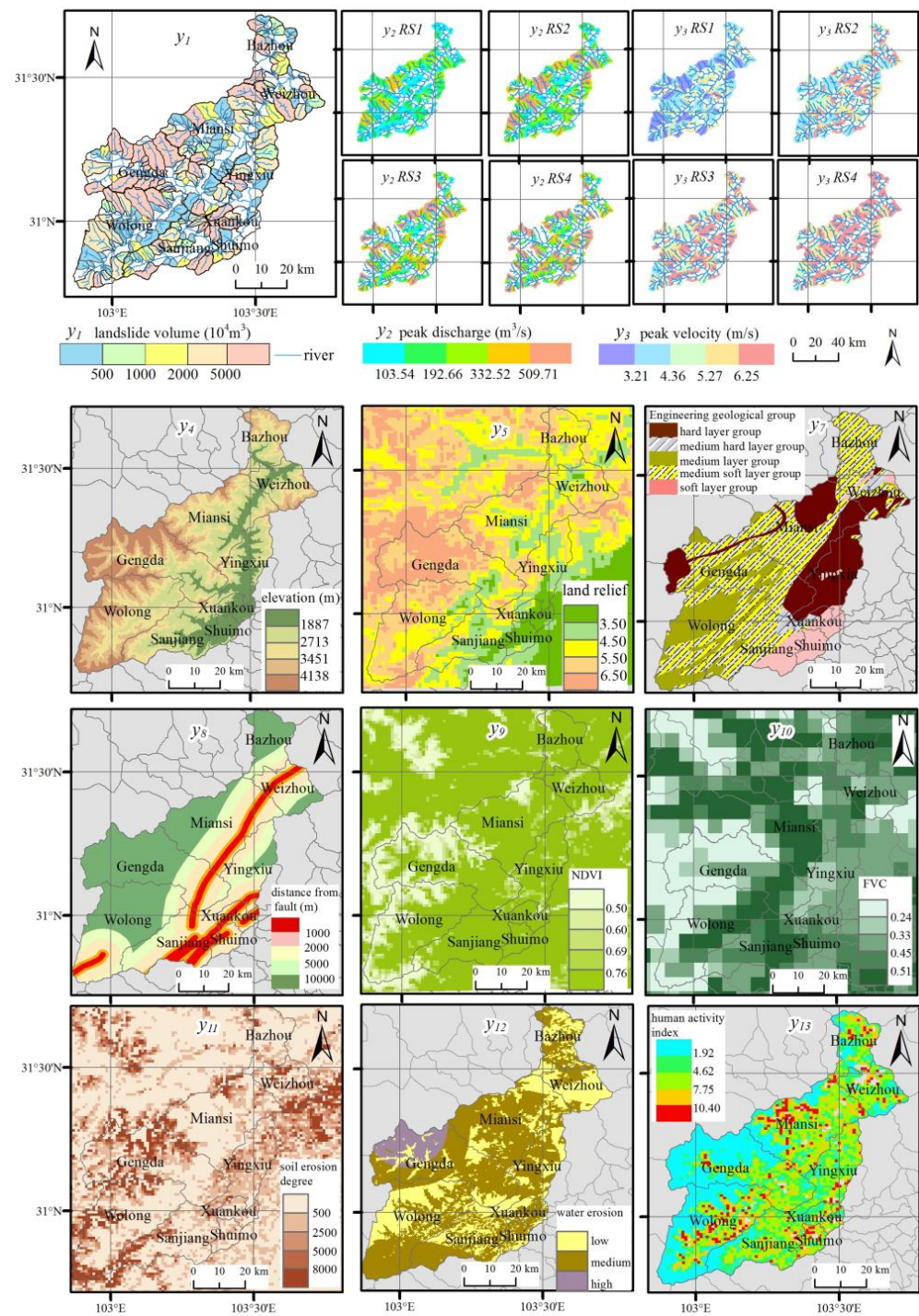


Figure 3. Classification of the hazard factors of debris flows. In the sub-figure “engineering ecological group”, the hard layer group includes granite, gabbro, breccia, and diorite. The medium-hard layer group mainly consists of dolomite and marble. The medium layer group includes slate, limestone, and clausolite. The medium-soft layer group consists of tuff, phyllite, marl, and siltstone. The soft layer group includes mudstone and shale.

4.1.2. Debris Flow Hazard Analysis

The total debris flow hazard area in Wenchuan is 425.12 km², and the radius of the alluvial fan is 0.20–0.65 km (Figure 4). The areas in Wolong and Gengda are relatively high at 88.12 km² and 84.93 km², respectively, while those in Shuimo and Xuankou are lower at 2.78 km² and 5.87 km², respectively, due to difficulties in delimiting the gully areas in the mainstream area of the Minjiang River. Using the indicator system for debris flows, the

results of the regional hazards were obtained (Figure 4). In the potential area, the average hazard gradually increases with rainstorm intensity; and the values under scenarios RS1, RS2, RS3, and RS4 are 0.25, 0.37, 0.49, and 0.57, respectively. This value is generally low under scenario RS1, ranging from 0.14 to 0.35. Under scenario RS4, the regional debris flow hazard is 0.34–0.78, and 60.31% of the hazard area is higher than 0.5. The hazard in Miansi, Shuimo, and Xuankou in the southwestern part of the study area is significantly higher, with the highest increment of 0.12.

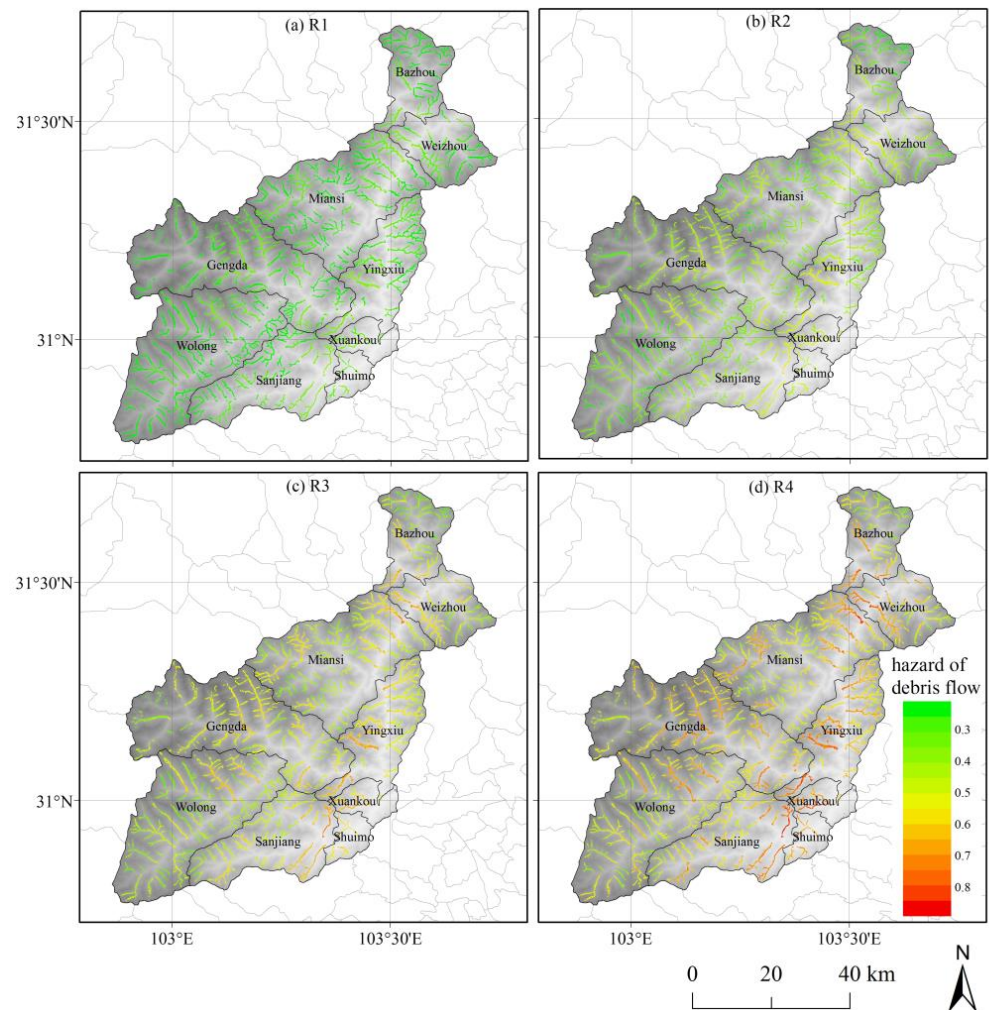


Figure 4. Spatial analysis of the debris flow hazards under rainstorm scenarios.

From the perspective of the distribution of the debris flow hazard at the township scale (Figure 5), it is relatively high in Xuankou (0.32, 0.47, 0.62, and 0.74 under scenarios RS1, RS2, RS3, and RS4, respectively) where there are fewer hazard areas. It is 0.22, 0.34, 0.44, and 0.52 in Wolong, which has the largest hazard area. As the intensity of the heavy rain increases, the hazard increases significantly, but the growth rate decreases. The debris flow hazard under scenario RS2 in the township increases by 0.11–0.15, and the growth rate is 47.65–51.00% compared with scenario RS1. The hazard under scenario RS4 increases by 0.07–0.12, and the growth rate is 15.72–19.26% compared with scenario RS3. From the perspective of the hazard anomaly percentage of each township, Xuankou, Shuimo, and Yingxiu are significantly higher than the regional average; Gengda, Sanjiang, and Weizhou are slightly higher; Bazhou and Wolong are lower.

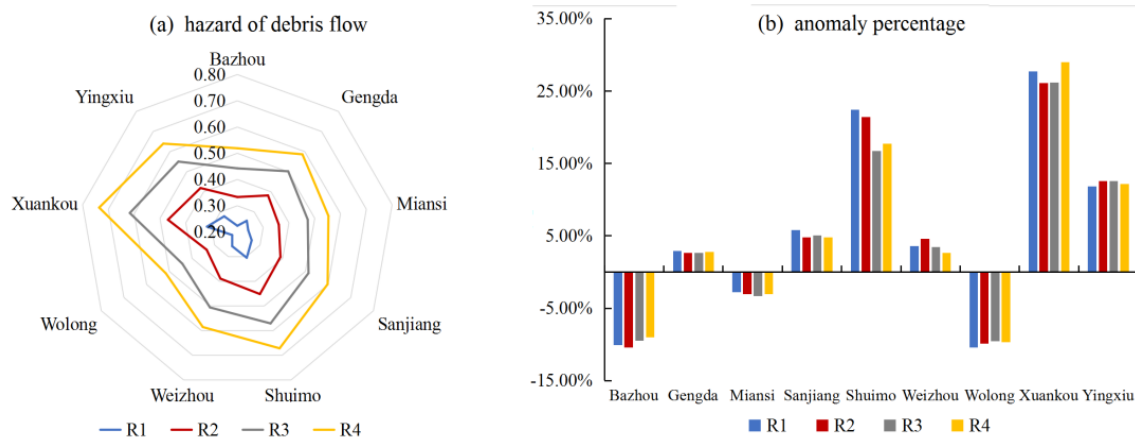


Figure 5. The debris flow risk statistics at the township scale under the four rainstorm scenarios.

4.2. Risk of Population Loss Due to the Disaster Chain in Wenchuan County

4.2.1. Risk of Earthquake-Landslide-Debris Flow Disaster Chain

According to the improved risk assessment method, the population loss risks posed by an earthquake-landslide-debris flow disaster chain under the Wenchuan Ms8.0 earthquake and four rainstorm scenarios were evaluated (Figure 6). The risks of population loss are 10,579, 10,761, 10,928, and 11,045 people (when the population risk is measured in people, less than 1 is counted as 1) under scenarios RS1, RS2, RS3, and RS4, respectively. The regional average risk is 2.59 people/km², 2.64 people/km², 2.68 people/km², and 2.71 people/km² under scenarios of RS1, RS2, RS3, and RS4, respectively, and these differences are mainly caused by the debris flow.

As the rainstorm intensity increases, the proportion of the population loss caused by the earthquake and landslides decreases, while the proportion caused by the debris flow increases significantly, with a growth rate of 119.22%. The population loss risk posed by the earthquake accounts for 57.76–55.32%, the landslide accounts for 38.82–37.18%, and the debris flow accounts for 3.42–7.50%. From the perspective of the spatial distribution, the risk in southeastern Wenchuan is significantly higher. In particular, the risks are relatively high in the high earthquake intensity area and the mountainous western area.

On the township scale, the population risks in Yingxiu, Gengda, and Miansi are relatively high at 3903, 2120, and 1062 people, accounting for 36.89%, 20.04%, and 10.03%, respectively, under scenario RS1. Yingxiu has the highest risk at 10.15 people/km², which is 3.90 times the regional average, followed by Xuankou and Weizhou at 7.86 people/km² and 3.21 people/km², respectively, and the risks in the other towns are lower than the average. As the rainstorm intensity increases, the population risk in the townships increases steadily. The proportions of the total population risk in Yingxiu, Gengda, Xuankou, and Sanjiang decrease mainly due to the low risk of debris flows in this region. The proportion in Yingxiu decreases by 1.23%, while the proportion in Weizhou increases significantly (1.12%).

The population loss rates (Figure 7) caused by an earthquake-landslide-debris flow disaster chain in Wenchuan are 9.06%, 9.21%, 9.35%, and 9.45% under rainstorm scenarios RS1, RS2, RS3, and RS4, respectively. For each element of the disaster chain, the population risk loss rate is 5.23% for the earthquake, 3.71% for the landslides, and 0.34%, 0.51%, 0.67%, and 0.78% for the debris flows under scenarios RS1, RS2, RS3, and RS4, respectively. At the township scale, all towns are strongly affected by the earthquake with a generally high population loss rate. Among them, Yingxiu Town is the most significant, which is located at the epicenter. The population loss rate of secondary geological disasters in Weizhou Town and Shuimo Town is relatively high. The population loss rate in Yingxiu is 25.82–26.07%, of which the earthquake population loss rate is 23.74%. The population loss rates caused by debris flows in Weizhou under scenarios RS3 and RS4 (2.38% and 2.75%, respectively) are higher than those caused by landslides. The mortality rates are

greatly affected by landslides in Shuimo, Bazhou, and Wolong, with loss rates of 1.69%, 4.59%, and 2.29%, respectively. In addition to the relatively high population risks posed by landslides in Shuimo and Wolong, the population loss rates caused by debris flows under a high rainstorm intensity are 0.86% and 0.42% in Shuimo and Wolong, respectively, which exceed the risks posed by an earthquake.

According to the statistical results of the risks under different earthquake intensities (Table 4), the population risk and loss rate of the disaster chain increase as the earthquake intensity increases. For example, as earthquake intensity increases, the population loss risks increase from 1.16 people/km² to 10.17 people/km², and the loss rates increase from 4.52% to 29.28% under scenario RS1. For the elements of the disaster chain, the loss rate caused by the earthquake increases the most significantly with increasing earthquake intensities, while those caused by the landslides and debris flows fluctuate. The population loss caused by the earthquake is the highest under intensities X and XI, followed by that caused by landslides, and that caused by debris flows is the lowest. In the IX and VIII intensity zones, the landslides and debris flows have relatively high risks, and the earthquake risk is relatively low. Under intensity XI, the loss rate caused by an earthquake is the highest (26.67%), and that caused by landslides is the lower (3.27%). Under intensity VIII, the population loss rate caused by landslides and debris flows is higher than that caused by the earthquake, i.e., 4.15% and 0.29–0.66%, respectively.

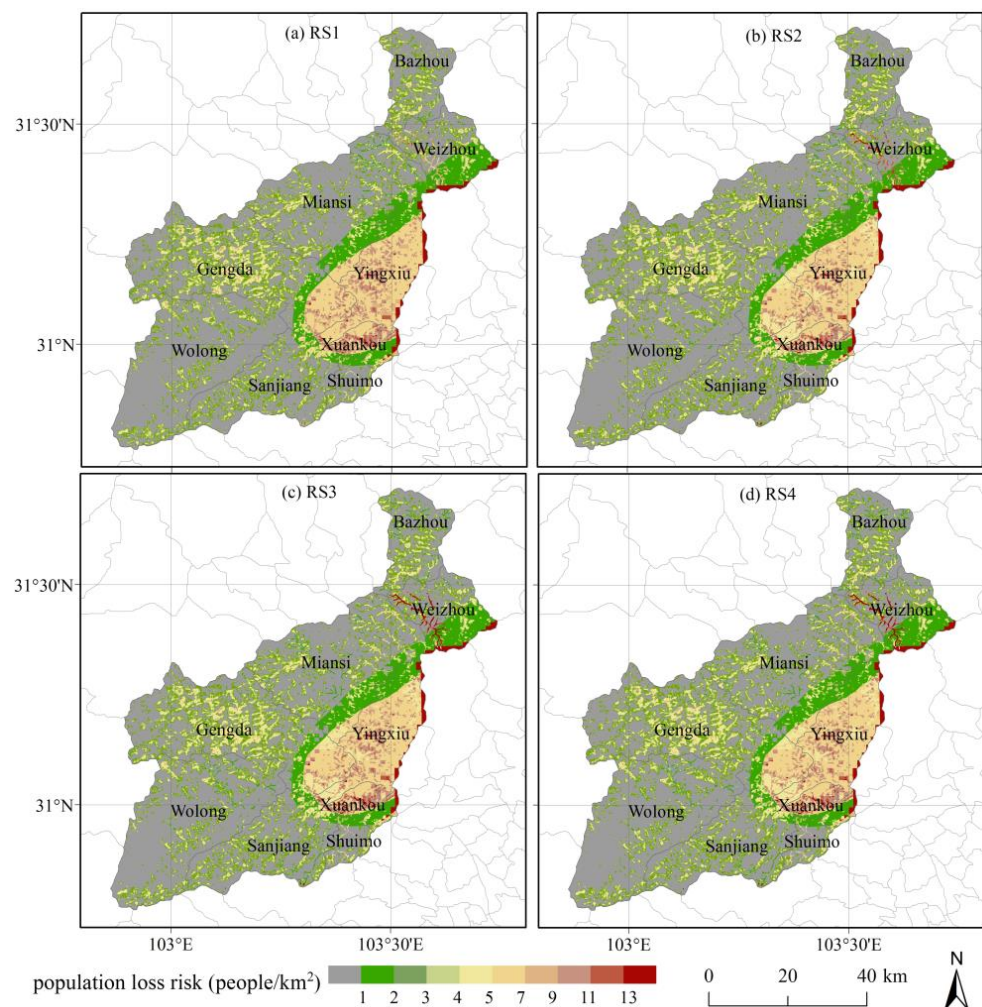


Figure 6. Spatial analysis of the population risk posed by an earthquake-landslide-debris flow disaster chain under the four rainstorm scenarios.

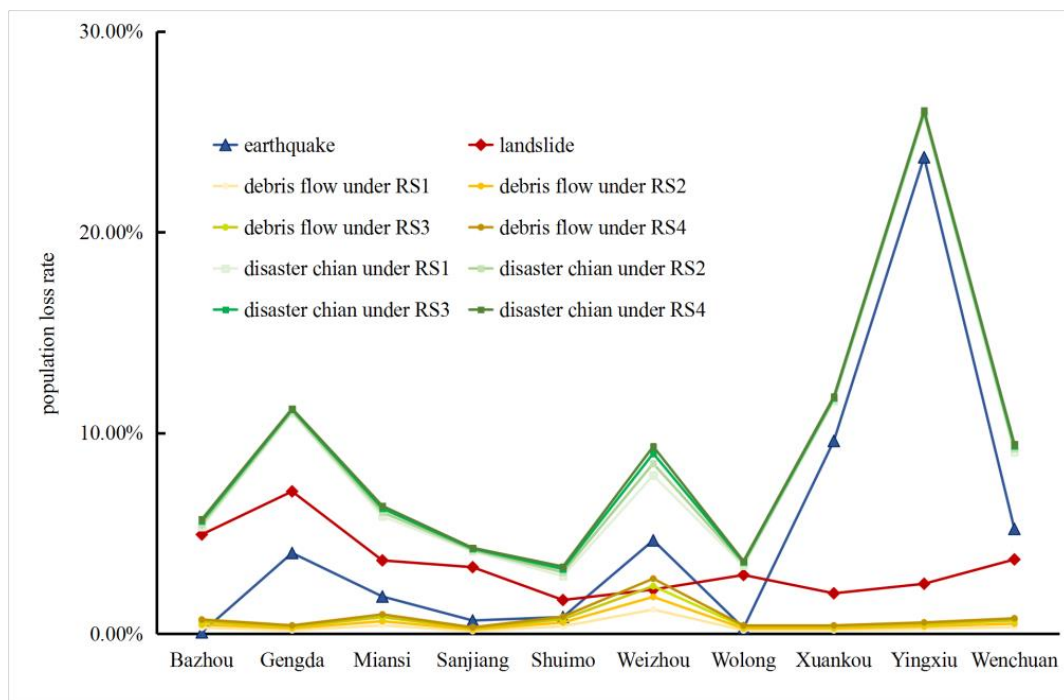


Figure 7. Comparison of the population loss rate caused by an earthquake-landslide-debris flow disaster chain in the different townships.

Table 4. Population loss risks and rates caused by a disaster chain under different earthquake intensities.

Earthquake Intensity	VIII		IX		X		XI	
	Risk (people/km ²)	Rate (%)						
Earthquake	0.03	0.10	0.15	0.61	2.56	6.05	9.26	26.67
Landslide	1.07	4.15	1.10	4.40	0.72	1.80	0.83	3.27
Debris flow under RS1	0.07	0.29	0.10	0.40	0.15	0.39	0.08	0.31
Debris flow under RS2	0.11	0.43	0.14	0.60	0.24	0.61	0.11	0.46
Debris flow under RS3	0.14	0.56	0.19	0.78	0.31	0.78	0.15	0.60
Debris flow under RS4	0.16	0.66	0.22	0.91	0.36	0.91	0.17	0.71
Disaster chain under RS1	1.16	4.52	1.35	5.37	3.43	8.11	10.17	29.28
Disaster chain under RS2	1.20	4.65	1.40	5.55	3.52	8.31	10.21	29.39
Disaster chain under RS3	1.23	4.78	1.44	5.72	3.59	8.47	10.24	29.49
Disaster chain under RS4	1.25	4.87	1.47	5.85	3.64	8.59	10.27	29.57

The population loss risk posed by the earthquake-landslide-debris flow disaster chain was analyzed using probability statistics at an interval of 0.5 (Figure 8). As the risk value increases, the corresponding probability value decreases, and the rate of decrease of the frequency under scenario RS1 is larger than those under the other scenarios. The frequencies of risks of less than 1.0 person/km² are 0.53, 0.52, 0.51, and 0.50 under scenarios RS1, RS2, RS3, and RS4, respectively. When the risk is higher than 3.5 people/km², the frequencies are 0.26, 0.27, 0.28, and 0.28, respectively. In the RS1 heavy rain scenario, as the risk increases, the rate for the frequency reduction is more obvious. According to the curve fitting, when the risk of population loss is lower, the lower the rainfall intensity, the higher the risk frequency. By contrast, when the risk is higher, the frequency is higher under the higher rainfall intensity scenario.

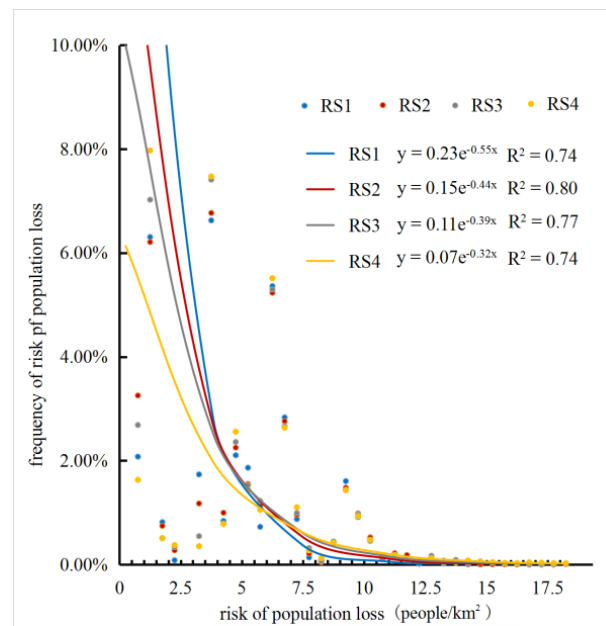


Figure 8. The probability distribution and curve fitting of the population loss risk posed by the disaster chain.

4.2.2. Population Loss Risk Posed by Each Element of the Disaster Chain

Under the Wenchuan Ms8.0 earthquake scenario, the population loss risk posed by the Wenchuan earthquake is 1.5 people/km² (Figure 9). It is higher in areas with an earthquake intensity of XI, with an average value of 9.61 people/km². It is 1.89 people/km², 0.16 people/km², 0.02 people/km² in the areas with earthquake intensities of X, IX, and VIII, respectively. At the township scale, the risks in Yingxiu, Xuankou, and Weizhou are higher than the average risk level in the study area. It is highest in Yingxiu (9.29 people/km²), followed by Xuankou (6.51 people/km²) and Weizhou (1.90 people/km²). Bazhou is mainly located in the VIII zone and has the lowest risk (0.02 people/km²). Under the Wenchuan Ms8.0 earthquake scenario, the population exposure of the landslide was 27.16 people/km² after 6111 people were lost during the earthquake. The risk of population loss posed by the landslides in Wenchuan is 1.01 people/km². The risks in Sanjiang, Gengda, Bazhou, and Xuankou are higher than the average risk level in the study area, at 1.10 people/km², 1.53 people/km², 1.15 people/km², and 1.23 people/km², respectively, while the risk in Wolong is the lowest (0.69 people/km²).

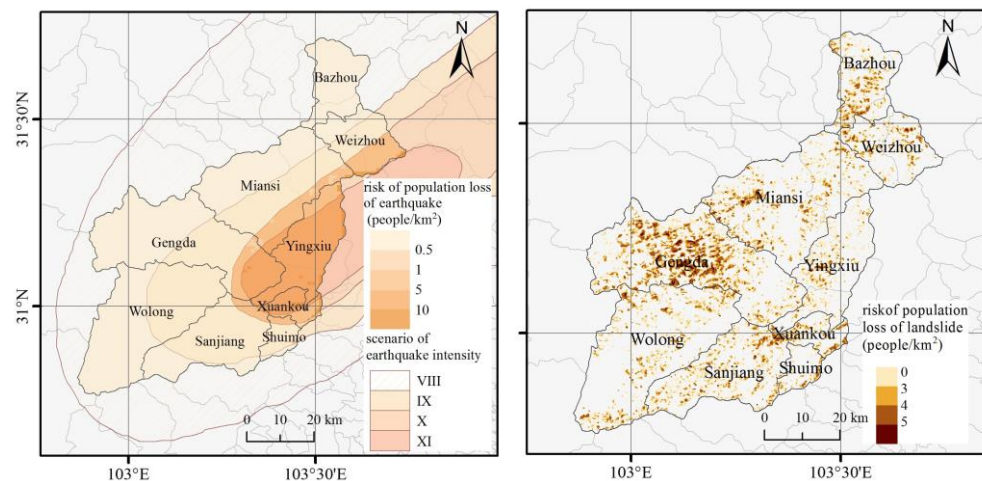


Figure 9. Spatial analysis of the population loss risks posed by the earthquake and landslides under the Ms8.0 earthquake scenario.

From the perspective of an earthquake-landslide disaster chain (Figure 10), the population loss risk in the study area is 10,217 people (2.51 people/km^2), with relatively high values in Yingxiu and Xuankou ($10.04 \text{ people/km}^2$ and 7.75 people/km^2 , respectively). The earthquake and landslides accounted for 59.80% and 40.20%, respectively, of the risk posed by this disaster chain. As the earthquake intensity increases, the risk posed by the earthquake increases significantly, but the risk posed by the landslides in the lower-intensity areas increases even more significantly than the earthquake risk. The earthquake-landslide disaster chain risk in the XI zone is $10.09 \text{ people/km}^2$, and the risk posed by the earthquake accounts for 91.76%, which is significantly higher than that caused by the landslides. The risk in the VIII zone is 1.10 people/km^2 , and the risk posed by the earthquake accounts for 2.37%, while that posed by the landslides accounts for 97.63%.

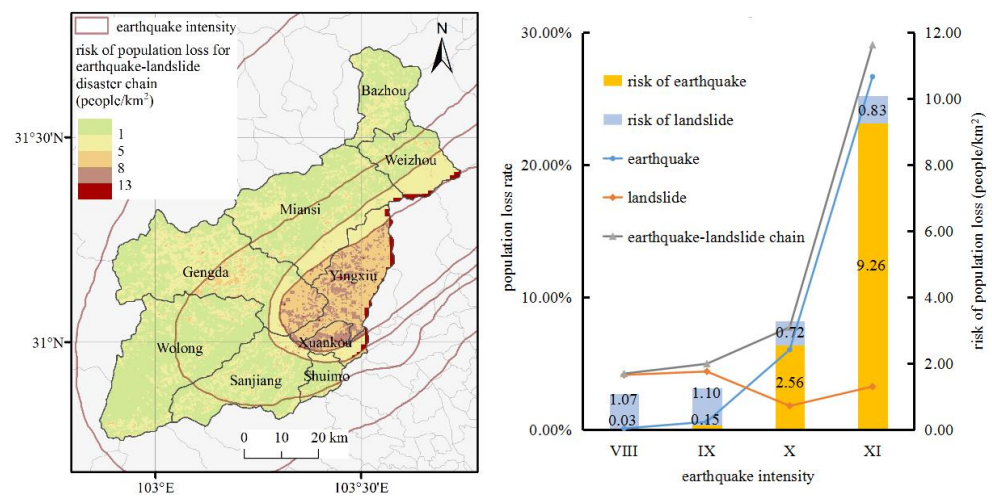


Figure 10. The risk and rate of population loss posed by the earthquake-landslide disaster chain in Wenchuan.

The population loss risks posed by debris flows in Wenchuan are 0.09 person/km^2 , 0.13 person/km^2 , 0.17 person/km^2 , and 0.20 person/km^2 under rainstorm scenarios (Figure 11). As the intensity of the heavy rains increases, the risk of population loss posed by debris flows increases steadily, and the frequency of the higher risk of population loss increases. Under scenario RS1, the regional population loss risk posed by debris flows is mainly $0.20\text{--}0.60 \text{ people/km}^2$, of which 40.31% of the debris flow valley area has a risk of fewer than 0.40 people/km^2 and 78.86% of the debris flow valley has a risk of fewer than 0.60 people/km^2 . Under scenario RS4, 70.56% of the debris flow valley area has a risk of $0.60\text{--}1.20 \text{ people/km}^2$ and 48.39% of the debris flow valley area has a risk of greater than 1 person/km^2 . At the township scale, the debris flow risks in Weizhou, Shuimo, Xuankou, and Miansi are higher than the regional average. The debris flow risk in Weizhou is relatively high, at 0.46 people/km^2 , 0.70 people/km^2 , 0.90 people/km^2 , and 1.04 people/km^2 under rainstorm scenarios. The risk in Gengda is the lowest, at 0.04 people/km^2 , 0.06 people/km^2 , 0.07 people/km^2 , and 0.09 people/km^2 , respectively.

4.3. Verification of the Risk Assessment Results

In this study, information obtained from the literature showed that the population loss in Wenchuan was 15.94 thousand people for the earthquake events in 2008. The population risk posed by the earthquake-landslide-debris flow disaster chain was about 11.00 thousand people in this paper, which is not significantly different from the actual data. Moreover, the population risk posed by debris flows was compared with data for several debris flow events to verify the reliability of the simulation results (Table 5). The results are in good agreement with the actual losses or casualties caused by events in several gullies. For example, a debris flow in Taoguan Gully in 2013 lost 1 person, while the simulation results provided a risk of $0.53\text{--}1.31$ people under the different rainstorm scenarios. A debris

flow disaster in Yaozi Gully in 2019 lost seven people, while the simulation results were 5.58–13.75 people.

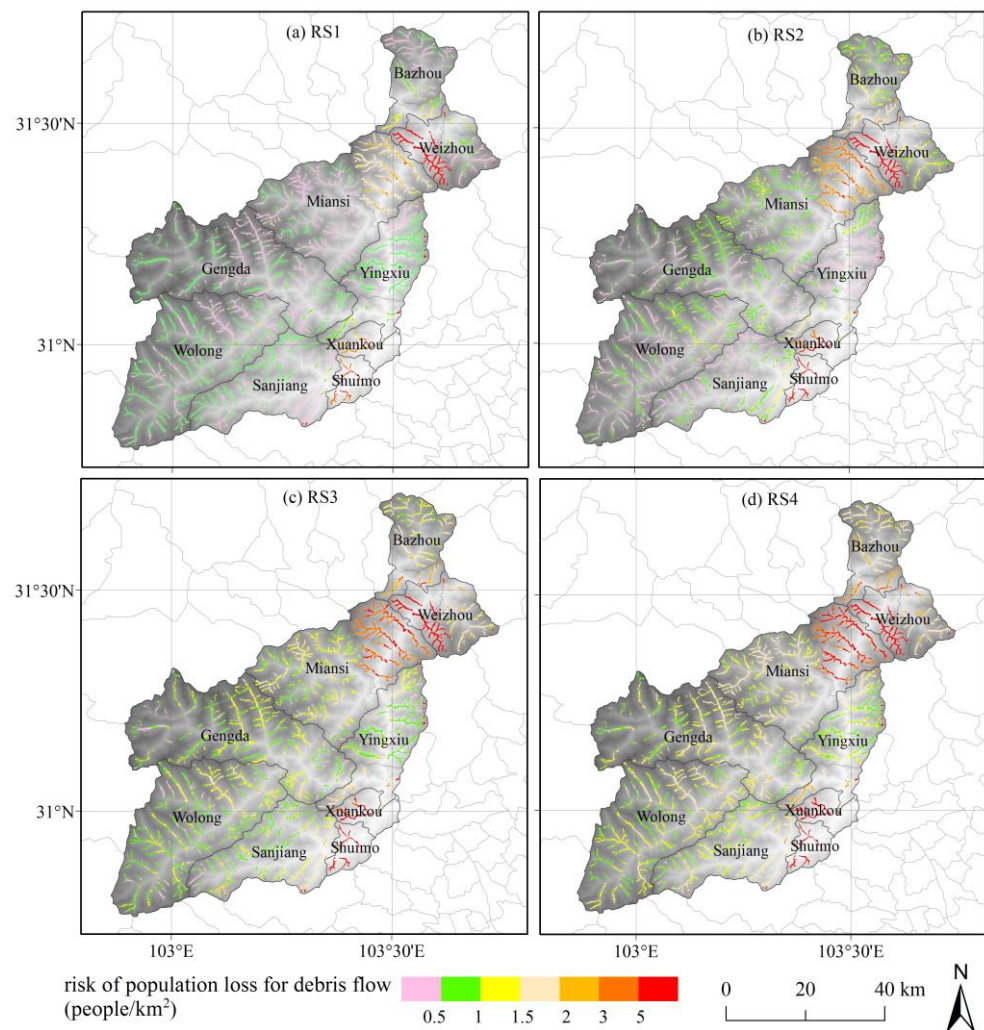


Figure 11. Spatial distribution of the population loss risks posed by debris flows in Wenchuan under the four rainstorm scenarios.

Table 5. Comparison of the simulated and actual population losses caused by debris flows.

Disaster Events	Actual Population Loss or Casualty (People)	Risk of Population Loss (People)			
		RS1	RS2	RS3	RS4
Huaxi Gully	1	1.81	2.60	3.41	3.88
Taoguan Gully	1	0.53	0.84	1.15	1.31
Jie Village	2	1.78	2.62	3.45	4.03
Yaozi Gully	7	5.85	8.82	11.70	13.75
Kechong Village	2	1.81	2.60	3.41	3.88
Cutou Gully	3	5.33	7.91	10.51	12.37

5. Discussion

5.1. Reliability of Population Risk for the Disaster Chain

The risk assessment results of this study were verified through comparison with data for actual disaster events, indicating that the method proposed in this study has a certain scientific value for risk assessment of earthquake-landslide-debris flow disaster chains. However, the accuracy of the risk results in some gullies needs to be improved which may

be related to regional disaster prevention and mitigation measures [41,71]. In 2013, the population loss caused by a debris flow in Qipan Gully was 15 people, including 13 tourists and 2 workers [72]. However, the simulation results indicated 82–188 people, which is much higher than the actual value. This discrepancy may be related to the timely implementation of emergency measures [71]. In 2019, 15 people were lost in a debris flow in Zhaobi Village, but the simulation results were slightly lower (4–8 people). During this disaster event, village officials strengthened inspections after heavy rains, carried out monitoring and prevention measures, and the timely relocation of villagers to safer areas. There were no deaths in some gullies in Qiangfeng, mainly due to timely weather warnings, monitoring, and population relocation [34,72]. Risk assessment for disaster chains is closely related to regional risk management and prevention. Therefore, considering the interactions between the current regional disaster prevention and the disaster scenarios in the risk assessment process is of great significance for enhancing the reliability of future risk assessments.

The population loss risk posed by an earthquake-landslide-debris flow disaster chain simulated in this paper is about 11.00 thousand people, including the risks posed by the earthquake, landslides, and debris flows, which occurred at different times and sequentially. There is still some data gap that may be caused by the occurrence of a large number of other co-seismic disasters (dammed lakes, floods, etc.), or may be related to errors in the risk assessment [73]. The results show that the risks posed by landslides in high earthquake intensity areas may be lower than those in low earthquake intensity areas, which may be related to the influence of the regional geological conditions and the errors in the existing earthquake-landslide hazard assessments [41,74]. In view of the uncertainty of regional risk results, factor analysis methods can be further used to explore the sensitivity of risks to topography, environment, and other factors to further clarify the characteristics of disaster chain risks [63,64,75]. In summary, it would be valuable to collect more disaster data, strengthen field investigations, and improve research on mechanism processes and verify the simulation results from multiple aspects [63,64,75].

In this study, the earthquake intensity used the classification result based on Chinese standards to analyze risks [11,51]. The measurements of earthquake intensity scales have great influences on earthquake prevention and disaster mitigation [76]. Many earthquake intensity scales have been used around the world, such as Environmental Seismic Intensity (ESI) [12,13,77], European Microseismic Scale (EMS) [14], the Chinese seismic intensity scale [11], shake map in America [78], Japan Meteorological Agency (JMA) Instrumental Seismic Intensity [79], etc. There are some differences between these classifications of earthquake intensity. ESI mainly considers earthquake environmental effects and quantifies the size and distribution of some disasters such as landslides and tsunamis [77]. EMS and Chinese standards have 2–3 quantitative terms of damage degree for each type of house in each intensity, but there are differences in the description of house type and earthquake damage degree [11,14]. The earthquake intensity of JMA is divided by 8 degrees, and the quantification related to house damage is rarely mentioned [79]. The shake map uses instrument monitoring data to estimate the earthquake intensity based on empirical formulas. These methods and standards will result in different intensity values. However, basic seismic data (such as house damage), which is necessary to estimate the results of the earthquake intensity according to different scales, is difficult to obtain. Earthquake intensity scales are also constantly being developed [79,80]. In the future, regional risks can be further studied according to different earthquake intensity scales to enhance the comparability of research results on a global scale.

5.2. Limitations on Hazard Assessment of Debris Flows

In this study, the hazard posed by a debris flow is based on multiple indicators, and the weight and classification of each factor may lead to controversy because the thresholds of the classifications may not apply to all gullies. Rainfall intensity is an important factor to be discussed since it is related to the intensity of debris flows [81]. The amount of precipitation recorded during different debris flow events fluctuates within a

relatively large range, usually ranging from 4.3 to 75.2 mm/h [68,70,82]. Therefore, relevant monitoring data should be established or improved, and the classification threshold should be further clarified in future studies. Moreover, in the context of climate change, the scale and frequency of extreme rainstorm events have increased, and the impact of geological disasters has also expanded. Therefore, it is necessary to carry out the risk assessment of geological disasters affected by climate change to reduce the potential loss induced by meteorological factors [37,61].

As for the study of debris flow hazard areas, empirical formulas from previous studies were used to delimit the alluvial fans. At present, related functional equations (such as the functional relationship between the run-out distance of the debris flow, the scale of the debris flow, and the height difference) are commonly constructed using statistical regression methods [48,83,84]. Studies have also been conducted to estimate the temporal and spatial distributions of alluvial fans using numerical simulation methods [16,81,85]. Therefore, more factors, such as the rainstorm intensity, should be considered to simulate the hazard area more accurately and to provide a more scientific basis for risk assessment research.

Some parameters were used to evaluate the debris flow factors. For example, the density of the debris flow is highly correlated with the recurrence period of the rainfall and the deposits [70,86]. The amplification coefficient usually ranges from 0.3 to 0.8, but it is 1.92 in some studies that took into account the intensity of short-duration rainstorms and the particular characteristics of the earthquake area [87]. The obstructive coefficient is generally 1.1–2.5, but can also range from 2.5 to 5 when a large amount of accumulated materials is considered [30]. As the rainstorm intensity increases, the debris flow may transform from a general type to a dam-breaking type, and thus, the amount of the breaking maybe dozens or even hundreds of times larger [57]. It is difficult to directly set the parameters and test the reliability for lots of debris flows because the existing data and studies are mostly based on the statistics of and prediction data for general types. Further studies with refined parameters can provide a theoretical basis for such debris flows that occur after an earthquake.

5.3. Uncertainties in the Vulnerability Curves or Indices

The population's vulnerabilities to earthquakes, landslides, and debris flows have mainly been studied using surface, curve, matrix, and coefficient in existing studies [51–53,88–90]. The determination of the vulnerability to earthquakes mostly uses an empirical formula that considers the epicentral intensity and the entire population affected while there is difficulty converting between the epicentral intensity and the earthquake intensity [11,51]. The determination of the vulnerability to landslides usually involves using key factors such as the hazard, depth, and impact pressure to construct a mortality curve [31,88]. The vulnerability to debris flows is based on the parameters at the administrative unit scale based on parameters such as the age structure of the population. In addition, the eruption characteristics of the debris flow and the natural conditions can also be considered [91]. However, the lithology is not considered in the vulnerability curve according to [52] because it may be a complex work because of difficulties in obtaining the loss rate of each lithology. As a large amount of data is not generally available, many studies refer to the vulnerability results of existing studies and have a reference value. In recent years, in the context of future population growth and climate change, and due to the continuous attention paid to the uncertainty of the vulnerability assessment, innovative equipment, and risk assessment, further research on the analysis and quantification of population vulnerability is very important for regional disaster prevention and mitigation [37,90].

6. Conclusions

The earthquake-landslide-debris flow disaster chain in Wenchuan poses a huge threat to the population. Population loss risk assessment is conducive to disaster reduction in advance and reduces the number of fatalities. Based on the cascading effect of this disaster chain, this study focused on the influence of the landslide volume and rainstorm intensity

on debris flows and assess the population loss risk posed by each element of the disaster chain. The main conclusions are as follows.

(1) The population loss risks posed by an earthquake-landslide-debris flow disaster chain are 2.59 people/km², 2.64 people/km², 2.68 people/km², and 2.71 people/km² under scenarios RS1, RS2, RS3, and RS4, respectively. For the elements of the disaster chain, the risk posed by the earthquake accounts for the highest proportion (57.76–55.32%), and that posed by the debris flow accounts for the lowest proportion. As the rainstorm intensity increases, the hazard and risk posed by debris flows increase steadily, and the frequency of higher risks of population loss increases.

(2) The population risk and loss rates caused by the disaster chain increase as the earthquake intensity increases. The loss rate caused by the earthquake increases most significantly (0.10–26.27%) with increasing earthquake intensity, and those caused by the landslides and debris flows fluctuate. The population loss caused by the earthquake is the highest in the high earthquake intensity zones; in the lower intensity zones, landslides and debris flows pose relatively high risks.

(3) The simulation results in this study assess the population risk posed by a regional disaster chain well based on a comparison between the simulated population loss risk and data for actual disaster events. By reducing the uncertainty of the comparison results, the debris flow risk assessment, and the population vulnerability, the reference value of the risk assessment method for disaster chains and for estimating future risks can be further improved.

Author Contributions: Conceptualization, Xiang Han, Yunhe Yin, and Shaohong Wu; methodology, Xiang Han and Yunhe Yin; software, Xiang Han and Yuming Wu; validation and resources, Yuming Wu, Shaohong Wu, and Xiang Han; writing, review and editing, Xiang Han and Yunhe Yin; supervision, Yuming Wu and Shaohong Wu. All authors have read and agreed to the published version of the manuscript.

Funding: This research was funded by the National Key R&D Program of China, grant number 2018YFC1508805, and the Strategic Priority Research Program of the Chinese Academy of Sciences, grant number XDA19040304.

Data Availability Statement: The data presented in this study are available from the author upon reasonable request.

Acknowledgments: The authors would like to thank the reviewers for their helpful suggestions and comments. The authors would like to express sincere appreciation to Xiliu Yue for some data and to acknowledge the data support from National Earth System Science Data Center, National Science & Technology Infrastructure of China (<http://www.geodata.cn> (accessed on 15 May 2020)), National Tibetan Plateau Data Center (<https://data.tpdc.ac.cn/> (accessed on 15 May 2020)), and Resource and Environment Science and Data Center (<http://www.resdc.cn/> (accessed on 15 May 2020)).

Conflicts of Interest: The authors declare no conflict of interest.

References

1. Ward, P.J.; Blauhut, V.; Bloemendaal, N.; Daniell, J.E.; De Ruiter, M.C.; Duncan, M.J.; Emberson, R.; Jenkins, S.F.; Kirschbaum, D.; Kunz, M.; et al. Review article: Natural hazard risk assessments at the global scale. *Nat. Hazards Earth Syst. Sci.* **2020**, *20*, 1069–1096. [[CrossRef](#)]
2. Mazzorana, B.; Simoni, S.; Scherer, C.; Gems, B.; Fuchs, S.; Keiler, M. A physical approach on flood risk vulnerability of buildings. *Hydrol. Earth Syst. Sci.* **2014**, *18*, 3817–3836. [[CrossRef](#)]
3. AghaKouchak, A.; Huning, L.S.; Chiang, F.; Sadegh, M.; Vahedifard, F.; Mazdiyasn, O.; Moftakhari, H.; Mallakpour, I. How do natural hazards cascade to cause disasters? *Nat. Cell Biol.* **2018**, *561*, 458–460. [[CrossRef](#)] [[PubMed](#)]
4. UNISDR. Sendai Framework for Disaster Risk Reduction 2015–2030. 2015. Available online: https://www.preventionweb.net/files/43291_sendaiframeworkfordrren.pdf (accessed on 15 May 2020).
5. IRGC. *Risk Governance: Towards an Integrative Approach*; White Paper No. 1; IRGC: Geneva, Switzerland, 2005.
6. Zhang, Y.; Weng, W. A Bayesian Network Model for Seismic Risk Analysis. *Risk Anal.* **2021**. [[CrossRef](#)] [[PubMed](#)]
7. Fan, X.; Scaringi, G.; Korup, O.; West, A.J.; Van Westen, C.J.; Tanyas, H.; Hovius, N.; Hales, T.C.; Jibson, R.W.; Allstadt, K.E.; et al. Earthquake-Induced Chains of Geologic Hazards: Patterns, Mechanisms, and Impacts. *Rev. Geophys.* **2019**, *57*, 421–503. [[CrossRef](#)]
8. Petley, D. Global patterns of loss of life from landslides. *Geology* **2012**, *40*, 927–930. [[CrossRef](#)]

9. Dowling, C.A.; Santi, P.M. Debris flows and their toll on human life: A global analysis of debris-flow fatalities from 1950 to 2011. *Nat. Hazards* **2014**, *71*, 203–227. [[CrossRef](#)]
10. Khan, A.; Gupta, S.; Gupta, S.K. Multi-hazard disaster studies: Monitoring, detection, recovery, and management, based on emerging technologies and optimal techniques. *Int. J. Disaster Risk Reduct.* **2020**, *47*, 101642. [[CrossRef](#)]
11. Institute of Engineering Mechanics, CEA; Institute of Geophysics, CEA. *The Chinese Seismic Intensity Scale*; GB/T 17742-2008; Standards Press of China: Beijing, China, 2008; Volume 8.
12. Lekkas, E.L. The 12 May 2008 Mw 7.9 Wenchuan, China, Earthquake: Macroseismic Intensity Assessment Using the EMS-98 and ESI 2007 Scales and Their Correlation with the Geological Structure. *Bull. Seism. Soc. Am.* **2010**, *100*, 2791–2804. [[CrossRef](#)]
13. Lekkas, E. Macroseismicity and geological effects of the Wenchuan earthquake (MS 8.0R-12 May 2008), Sichuan, China: Macro-distribution and comparison of EMS1998 and ESI2007 intensities. *Bull. Geol. Soc. Greece* **2017**, *43*, 1361. [[CrossRef](#)]
14. Grünthal, G. *European Macroseismic Scale 1998*; Notebooks of the European Center for Geodynamics and Seismology; Council of Europe: Strasbourg, France, 1998.
15. Michetti, A.; Esposito, E.; Guerrieri, L.; Porfido, S.; Serva, L.; Tatevossian, R.; Vittori, E.; Audemard, F.; Azuma, T.; Clague, J.; et al. Environmental seismic intensity scale-ESI 2007. In *Memorie Descrittive della Carta Geologica d'Italia*; Guerrieri, L., Vittori, E., Eds.; Servizio Geologico d'Italia—Dipartimento Difesa del Suolo: APAT, Roma, Italy, 2007; Volume 74, pp. 7–54.
16. Zhang, Z.; Walter, F.; McArdell, B.W.; Wenner, M.; Chmiel, M.; De Haas, T.; He, S. Insights from the Particle Impact Model into the High-Frequency Seismic Signature of Debris Flows. *Geophys. Res. Lett.* **2021**, *48*, 2020–088994. [[CrossRef](#)]
17. Fan, X.; Juang, C.H.; Wasowski, J.; Huang, R.; Xu, Q.; Scaringi, G.; van Westen, C.J.; Havenith, H.-B. What we have learned from the 2008 Wenchuan Earthquake and its aftermath: A decade of research and challenges. *Eng. Geol.* **2018**, *241*, 25–32. [[CrossRef](#)]
18. Kappes, M.S.; Keiler, M.; von Elverfeldt, K.; Glade, T. Challenges of analyzing multi-hazard risk: A review. *Nat. Hazards* **2012**, *64*, 1925–1958. [[CrossRef](#)]
19. Gill, J.C.; Malamud, B.D. Reviewing and visualizing the interactions of natural hazards. *Rev. Geophys.* **2014**, *52*, 680–722. [[CrossRef](#)]
20. Shi, P.; Ye, T.; Wang, Y.; Zhou, T.; Xu, W.; Du, J.; Wang, J.; Li, N.; Huang, C.; Liu, L.; et al. Disaster Risk Science: A Geographical Perspective and a Research Framework. *Int. J. Disaster Risk Sci.* **2020**, *11*, 426–440. [[CrossRef](#)]
21. Li, Z.; Jiao, Q.; Liu, L.; Tang, H.; Liu, T. Monitoring Geologic Hazards and Vegetation Recovery in the Wenchuan Earthquake Region Using Aerial Photography. *ISPRS Int. J. Geo-Inf.* **2014**, *3*, 368–390. [[CrossRef](#)]
22. Han, L.; Zhang, J.; Zhang, Y.; Ma, Q.; Alu, S.; Lang, Q. Hazard Assessment of Earthquake Disaster Chains Based on a Bayesian Network Model and ArcGIS. *ISPRS Int. J. Geo-Inf.* **2019**, *8*, 210. [[CrossRef](#)]
23. Shieh, C.-F.; Sheu, S.-Y.; Shih, R.-C. Correlation between surface damage and the coseismic displacement and stress relaxation of the 1999 Chi-Chi, Taiwan Earthquake. *Geophys. Res. Lett.* **2001**, *28*, 3381–3384. [[CrossRef](#)]
24. King, T.R.; Quigley, M.C.; Clark, D. Earthquake environmental effects produced by the Mw 6.1, 20th May 2016 Petermann earthquake, Australia. *Tectonophysics* **2018**, *747–748*, 357–372. [[CrossRef](#)]
25. Liu, W.; Yang, Z.; He, S. Modeling the landslide-generated debris flow from formation to propagation and run-out by considering the effect of vegetation. *Landslides* **2021**, *18*, 43–58. [[CrossRef](#)]
26. Ni, H.; Tang, C.; Zheng, W.; Xu, R.; Tian, K.; Xu, W. An Overview of Formation Mechanism and Disaster Characteristics of Post-seismic Debris Flows Triggered by Subsequent Rainstorms in Wenchuan Earthquake Extremely Stricken Areas. *Acta Geol. Sin.* **2014**, *88*, 1310–1328. [[CrossRef](#)]
27. Sharma, K.; Saraf, A.K.; Das, J.; Baral, S.S.; Borgohain, S.; Singh, G. Mapping and Change Detection Study of Nepal-2015 Earthquake Induced Landslides. *J. Indian Soc. Remote Sens.* **2017**, *46*, 605–615. [[CrossRef](#)]
28. Serey, A.; Piñero-Feliciangeli, L.; Sepúlveda, S.A.; Poblete, F.; Petley, D.N.; Murphy, W. Landslides induced by the 2010 Chile megathrust earthquake: A comprehensive inventory and correlations with geological and seismic factors. *Landslides* **2019**, *16*, 1153–1165. [[CrossRef](#)]
29. Yagi, H.; Sato, G.; Higaki, D.; Yamamoto, M.; Yamasaki, T. Distribution and characteristics of landslides induced by the Iwate–Miyagi Nairiku Earthquake in 2008 in Tohoku District, Northeast Japan. *Landslides* **2009**, *6*, 335–344. [[CrossRef](#)]
30. Cui, P.; He, S.M.; Yao, L.K.; Wang, Z.Y.; Chen, X.Q. *Formation Mechanism and Risk Control of Geo-Disasters in Wenchuan Earthquake*; Science Press: Beijing, China, 2011.
31. Zhang, S.; Li, C.; Zhang, L.; Peng, M.; Zhan, L.; Xu, Q. Quantification of human vulnerability to earthquake-induced landslides using Bayesian network. *Eng. Geol.* **2020**, *265*, 105436. [[CrossRef](#)]
32. Xu, Q.; Zhang, S.; Li, W. Spatial distribution of large-scale landslides induced by the 5.12 Wenchuan Earthquake. *J. Mt. Sci.* **2011**, *8*, 246–260. [[CrossRef](#)]
33. Marc, O.; Hovius, N.; Meunier, P.; Uchida, T.; Hayashi, S. Transient changes of landslide rates after earthquakes. *Geology* **2015**, *43*, 883–886. [[CrossRef](#)]
34. Xiong, J.; Tang, C.; Chen, M.; Zhang, X.; Shi, Q.; Gong, L. Activity characteristics and enlightenment of the debris flow triggered by the rainstorm on 20 August 2019 in Wenchuan County, China. *Bull. Int. Assoc. Eng. Geol.* **2021**, *80*, 873–888. [[CrossRef](#)]
35. Chalkias, C.; Ferentinou, M.; Polykretis, C. GIS Supported Landslide Susceptibility Modeling at Regional Scale: An Expert-Based Fuzzy Weighting Method. *ISPRS Int. J. Geo-Inf.* **2014**, *3*, 523–539. [[CrossRef](#)]
36. Schmidt, J.; Matcham, I.; Reese, S.; King, A.; Bell, R.; Henderson, R.; Smart, G.; Cousins, J.; Smith, W.; Heron, D. Quantitative multi-risk analysis for natural hazards: A framework for multi-risk modelling. *Nat. Hazards* **2011**, *58*, 1169–1192. [[CrossRef](#)]

37. Gallina, V.; Torresan, S.; Critto, A.; Sperotto, A.; Glade, T.; Marcomini, A. A review of multi-risk methodologies for natural hazards: Consequences and challenges for a climate change impact assessment. *J. Environ. Manag.* **2016**, *168*, 123–132. [[CrossRef](#)] [[PubMed](#)]
38. Maskrey, A. Revisiting community-based disaster risk management. *Environ. Hazards* **2011**, *10*, 42–52. [[CrossRef](#)]
39. Korswagen, P.; Jonkman, S.; Terwel, K. Probabilistic assessment of structural damage from coupled multi-hazards. *Struct. Saf.* **2019**, *76*, 135–148. [[CrossRef](#)]
40. Zhou, H.-J.; Wang, X.; Yuan, Y. Risk assessment of disaster chain: Experience from Wenchuan earthquake-induced landslides in China. *J. Mt. Sci.* **2015**, *12*, 1169–1180. [[CrossRef](#)]
41. Wu, S.H.; Liu, Y.H.; Yue, X.L. *Risk Identification and Assessment of Seismic Geological Disaster Chain*; Science Press: Beijing, China, 2020.
42. Varnes, D.J. *Landslide Hazard Zonation: A Review of Principles and Practice (No. 3)*; UNESCO: Paris, France, 1984.
43. Zhou, J.-W.; Cui, P.; Yang, X.-G. Dynamic process analysis for the initiation and movement of the Donghekou landslide-debris flow triggered by the Wenchuan earthquake. *J. Asian Earth Sci.* **2013**, *76*, 70–84. [[CrossRef](#)]
44. Chang, M.; Tang, C.; Van Asch, T.W.J.; Cai, F. Hazard assessment of debris flows in the Wenchuan earthquake-stricken area, South West China. *Landslides* **2017**, *14*, 1783–1792. [[CrossRef](#)]
45. Gao, J.; Sang, Y. Identification and estimation of landslide-debris flow disaster risk in primary and middle school campuses in a mountainous area of Southwest China. *Int. J. Disaster Risk Reduct.* **2017**, *25*, 60–71. [[CrossRef](#)]
46. Wang, J.; He, Z.; Weng, W. A review of the research into the relations between hazards in multi-hazard risk analysis. *Nat. Hazards* **2020**, *104*, 2003–2026. [[CrossRef](#)]
47. Scheidl, C.; Rickenmann, D. Empirical prediction of debris-flow mobility and deposition on fans. *Earth Surf. Process. Landf.* **2009**, *35*, 157–173. [[CrossRef](#)]
48. Zhou, W.; Fang, J.; Tang, C.; Yang, G. Empirical relationships for the estimation of debris flow runout distances on depositional fans in the Wenchuan earthquake zone. *J. Hydrol.* **2019**, *577*, 123932. [[CrossRef](#)]
49. Department of Soil and Water Conservation. *Classification and Gradation Standard of Soil Erosion*; SL 190-2007, 26P; A25; China Water&Power Press: Beijing, China, 2008.
50. Xu, Y.; Xu, X.; Tang, Q. Human activity intensity of land surface: Concept, methods and application in China. *J. Geogr. Sci.* **2016**, *26*, 1349–1361. [[CrossRef](#)]
51. Wu, S.; Jin, J.; Pan, T. Empirical seismic vulnerability curve for mortality: Case study of China. *Nat. Hazards* **2015**, *77*, 645–662. [[CrossRef](#)]
52. Lin, Q.; Wang, Y.; Liu, T.; Zhu, Y.; Sui, Q. The Vulnerability of People to Landslides: A Case Study on the Relationship between the Casualties and Volume of Landslides in China. *Int. J. Environ. Res. Public Health* **2017**, *14*, 212. [[CrossRef](#)]
53. Ding, M.; Tang, C.; Huang, T.; Gao, Z. Dynamic Vulnerability Analysis of Mountain Settlements Exposed to Geological Hazards: A Case Study of the Upper Min River, China. *Adv. Civ. Eng.* **2020**, *2020*, 1–13. [[CrossRef](#)]
54. Yue, X.; Wu, S.; Yin, Y.; Gao, J.; Zheng, J. Risk Identification of Seismic Landslides by Joint Newmark and RockFall Analyst Models: A Case Study of Roads Affected by the Jiuzhaigou Earthquake. *Int. J. Disaster Risk Sci.* **2018**, *9*, 392–406. [[CrossRef](#)]
55. Wu, S.; Liu, L.; Gao, J.; Wang, W. Integrate Risk from Climate Change in China Under Global Warming of 1.5 and 2.0 °C. *Earth's Futur.* **2019**, *7*, 1307–1322. [[CrossRef](#)]
56. Zou, Q.; Cui, P.; Zeng, C.; Tang, J.; Regmi, A.D. Dynamic process-based risk assessment of debris flow on a local scale. *Phys. Geogr.* **2016**, *37*, 132–152. [[CrossRef](#)]
57. Fang, Q.; Tang, C.; Chen, Z.; Wang, S.; Yang, T. A calculation method for predicting the runout volume of dam-break and non-dam-break debris flows in the Wenchuan earthquake area. *Geomorphology* **2019**, *327*, 201–214. [[CrossRef](#)]
58. Li, L.; Yu, B.; Zhu, Y.; Chu, S.; Wu, Y. Topographical factors in the formation of gully-type debris flows in Longxi River catchment, Sichuan, China. *Environ. Earth Sci.* **2014**, *73*, 4385–4398. [[CrossRef](#)]
59. Basu, M. Gaussian-based edge-detection methods-a survey. *IEEE Trans. Syst. Man Cybern. Part C Appl. Rev.* **2002**, *32*, 252–260. [[CrossRef](#)]
60. Wang, N. *Prediction and Evaluation on Deposited Volume of Debris-Flow in Wenchuan Earthquake Area*; Chengdu University of Technology: Chengdu, China, 2015.
61. Li, M.; Tian, C.-S.; Wang, Y.-K.; Liu, Q.; Lu, Y.-F.; Shan, W. Impacts of future climate change (2030–2059) on debris flow hazard: A case study in the Upper Minjiang River basin, China. *J. Mt. Sci.* **2018**, *15*, 1836–1850. [[CrossRef](#)]
62. Niu, Q.; Cheng, W.; Liu, Y.; Xie, Y.; Lan, H.; Cao, Y. Risk assessment of secondary geological disasters induced by the Yushu earthquake. *J. Mt. Sci.* **2012**, *9*, 232–242. [[CrossRef](#)]
63. Ji, F.; Dai, Z.; Li, R. A multivariate statistical method for susceptibility analysis of debris flow in southwestern China. *Nat. Hazards Earth Syst. Sci.* **2020**, *20*, 1321–1334. [[CrossRef](#)]
64. Wu, S.; Chen, J.; Xu, C.; Zhou, W.; Yao, L.; Yue, W.; Cui, Z. Susceptibility Assessments and Validations of Debris-Flow Events in Meizoseismal Areas: Case Study in China's Longxi River Watershed. *Nat. Hazards Rev.* **2020**, *21*, 05019005. [[CrossRef](#)]
65. Cui, P.; Hu, K.; Zhuang, J.; Yang, Y.; Zhang, J. Prediction of debris-flow danger area by combining hydrological and inundation simulation methods. *J. Mt. Sci.* **2011**, *8*, 1–9. [[CrossRef](#)]
66. Hu, T.; Huang, R.-Q. A catastrophic debris flow in the Wenchuan Earthquake area, July 2013: Characteristics, formation, and risk reduction. *J. Mt. Sci.* **2017**, *14*, 15–30. [[CrossRef](#)]

67. Tang, C.; Zhu, J.; Li, W.L.; Liang, J.T. Rainfall-triggered debris flows following the Wenchuan earthquake. *Bull. Int. Assoc. Eng. Geol.* **2009**, *68*, 187–194. [[CrossRef](#)]
68. Zhou, W.; Tang, C. Rainfall thresholds for debris flow initiation in the Wenchuan earthquake-stricken area, southwestern China. *Landslides* **2014**, *11*, 877–887. [[CrossRef](#)]
69. Huang, H.; Yang, S.; Liu, J.; Yang, D.; Tian, Y. A study on the forecast calculating method of the density of rainfall debris flow in Southwestern of China. *Arab. J. Geosci.* **2020**, *13*, 1–11. [[CrossRef](#)]
70. Long, K.; Zhang, S.; Wei, F.; Hu, K.; Zhang, Q.; Luo, Y. A hydrology-process based method for correlating debris flow density to rainfall parameters and its application on debris flow prediction. *J. Hydrol.* **2020**, *589*, 125124. [[CrossRef](#)]
71. Tang, C.; Westen, C. *Atlas of Wenchuan-Earthquake Geohazards*; Science Press: Beijing, China, 2018.
72. China Institute of Water Resources and Hydropower Research. The Massive Debris Flow on 20 August 2019 in Wenchuan County, Sichuan Province. 2021. Available online: <http://www.qgshzh.com/ffpindex?newstype=1> (accessed on 4 August 2020).
73. China Association for Disaster Prevention. *Disaster Memorabilia in China*; Seismological Press: Beijing, China, 2008.
74. Wasowski, J.; McSaveney, M.; Pisano, L.; Del Gaudio, V.; Li, Y.; Hu, W. Recurrent rock avalanches progressively dismantle a mountain ridge in Beichuan County, Sichuan, most recently in the 2008 Wenchuan earthquake. *Geomorphology* **2021**, *374*, 107492. [[CrossRef](#)]
75. Xia, C.H.; Zhu, J.; Chang, M.; Yang, Y. Susceptibility assessment of debris flow using a probabilistic and GIS approach: A case study on the Wenchuan county. *J. Yangtze River Sci. Res. Inst.* **2017**, *34*, 34–38. (In Chinese)
76. Li, S.; Chen, Y.; Yu, T. Comparison of macroseismic-intensity scales by considering empirical observations of structural seismic damage. *Earthq. Spectra* **2021**, *37*, 449–485. [[CrossRef](#)]
77. Serva, L.; Vittori, E.; Comerci, V.; Esposito, E.; Guerrieri, L.; Michetti, A.M.; Mohammadioun, B.; Mohammadioun, G.C.; Porfido, S.; Tatevossian, R.E. Earthquake Hazard and the Environmental Seismic Intensity (ESI) Scale. *Pure Appl. Geophys.* **2016**, *173*, 1479–1515. [[CrossRef](#)]
78. Wald, D.J.; Quitoriano, V.; Heaton, T.H.; Kanamori, H. Relationships between Peak Ground Acceleration, Peak Ground Velocity, and Modified Mercalli Intensity in California. *Earthq. Spectra* **1999**, *15*, 557–564. [[CrossRef](#)]
79. Sokolov, V.; Furumura, T.; Wenzel, F. On the use of JMA intensity in earthquake early warning systems. *Bull. Earthq. Eng.* **2010**, *8*, 767–786. [[CrossRef](#)]
80. Naik, S.P.; Mohanty, A.; Porfido, S.; Tuttle, M.; Gwon, O.; Kim, Y.-S. Intensity estimation for the 2001 Bhuj earthquake, India on ESI-07 scale and comparison with historical 16th June 1819 Allah Bund earthquake: A test of ESI-07 application for intraplate earthquakes. *Quat. Int.* **2020**, *536*, 127–143. [[CrossRef](#)]
81. Liu, K.-F.; Li, H.-C.; Hsu, Y.-C. Debris flow hazard assessment with numerical simulation. *Nat. Hazards* **2008**, *49*, 137–161. [[CrossRef](#)]
82. Li, T.-T.; Huang, R.-Q.; Pei, X.-J. Variability in rainfall threshold for debris flow after Wenchuan earthquake in Gaochuan River watershed, Southwest China. *Nat. Hazards* **2016**, *82*, 1967–1980. [[CrossRef](#)]
83. Tang, C.; Zhu, J.; Chang, M.; Ding, J.; Qi, X. An empirical–statistical model for predicting debris-flow runout zones in the Wenchuan earthquake area. *Quat. Int.* **2012**, *250*, 63–73. [[CrossRef](#)]
84. Van Asch, T.W.J.; Tang, C.; Alkema, D.; Zhu, J.; Zhou, W. An integrated model to assess critical rainfall thresholds for run-out distances of debris flows. *Nat. Hazards* **2013**, *70*, 299–311. [[CrossRef](#)]
85. Ding, M.; Tang, C.; Miao, C. Response analysis of valley settlements to the evolution of debris flow fans under different topographic conditions: A case study of the upper reaches of Min River, China. *Bull. Int. Assoc. Eng. Geol.* **2019**, *79*, 1639–1650. [[CrossRef](#)]
86. Chen, X.; Chen, J.; Zhao, W.; Li, Y.; You, Y. Characteristics of a Debris-Flow Drainage Channel with a Step-Pool Configuration. *J. Hydraul. Eng.* **2017**, *143*, 04017038. [[CrossRef](#)]
87. Song, S.W. *Analysis and Investigation on Seismic Damages of Projects Subjected to Wenchuan*; Science Press: Beijing, China, 2009.
88. Pollock, W.; Wartman, J. Human Vulnerability to Landslides. *GeoHealth* **2020**, *4*, e2020GH000287. [[CrossRef](#)]
89. Totschnig, R.; Fuchs, S. Mountain torrents: Quantifying vulnerability and assessing uncertainties. *Eng. Geol.* **2013**, *155*, 31–44. [[CrossRef](#)]
90. Fuchs, S.; Keiler, M.; Ortlepp, R.; Schinke, R.; Papathoma-Köhle, M. Recent advances in vulnerability assessment for the built environment exposed to torrential hazards: Challenges and the way forward. *J. Hydrol.* **2019**, *575*, 587–595. [[CrossRef](#)]
91. Ding, M.; Huang, T. Vulnerability assessment of population in mountain settlements exposed to debris flow: A case study on Qipan gully, Wenchuan County, China. *Nat. Hazards* **2019**, *99*, 553–569. [[CrossRef](#)]